Elastic time-reverse modeling imaging conditions

Brad Artman[1]*, Igor Podladtchikov, and Alex Goertz, Spectraseis AG*

SUMMARY

Since the Earth is elastic, it is worth the computational burden to process multicomponent data for elastic phenomena with fully coupled time-domain wave-equation propagators. At every time sample in the back-propagated model domain, the complete wave field is decomposed exactly into compressional and shear wave components by simple spatial derivatives. Then, physically significant images are extracted from extrapolated hyper-cubes by applying appropriate imaging conditions. To locate subsurface sources (or diffractors) with the time-reverse modeling algorithm, the imaging condition required is the correlation of P and S energy since only at the source location are the two events collocated. The impulse response of the algorithm is anti-symmetric in physical space and can be enhanced through post-processing with a spatial derivative or integral.

SOURCE FOCUSING

The time-reverse modeling (TRM) algorithm was developed for locating sources within a model domain (Fink, 1999; Gajewski and Tessmer, 2005). The method is suited for locating earthquakes, microseismic events, or tremor sources. The difference between TRM and reverse-time migration (RTM) (Levin, 1984) is the lack of a known source wave field for TRM. Otherwise, *data* are treated in the same manner: reversed in time and used as source functions at the acquisition locations.

The difference between a specular reflection and a stimulated heterogeneity, or diffractor, is that data contain only a direct arrival ray path: The "from-path". This contrasts to reflection seismic whose time delays are the sum of the "to-path" and the "from-path." Without some knowledge of the to-path, imaging algorithms based on delays between a reference event and a scattering event, including RTM and interferometry, are incapable of finding sources within a domain. In contrast, the TRM algorithm exploits the ability to collapse travel-time surfaces (hyperbolic cones) using wave-equation propagators.

If data are collected as a function of time on a datum, the data space has dimensions (x,t). Using wave-equation extrapolators and a subsurface velocity model, we can create a depth axis to arrive at a hypercube with the original data dimensions and an extra spatial model dimension associated with propagation. Figure 1 shows the simple kinematic surface of an energy source within a mixed model-data domain. The extrapolation direction is defined as z, but of course could be any model domain vector. The (x,t) data recorded on the acquisition datum is a hyperbola for a homogeneous medium. The (x,z) position of the source is at the intersection of the two symmetric cones. Acausal propagation of the data, or causal propagation of time-reversed data, will collapse moveout in the data to the location of the source and then unfocus that point with subsequent extrapolation steps. Of course, the travel-time surface in Figure 1 is only a single order-zero solution to the full elastic wave equation: far field, single mode, constant velocity, etc.

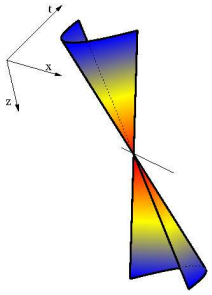

Figure 1 Simplified propagation surface in the combined data-model domain. Source location is at the intersection of the two cones. Cool colors reflect decreased amplitude due to geometric spreading.

Since the time and depth dimensions of the hypercube are redundant, an imaging condition which collapses the time axis provides an image defined by purely spatial coordinates. Defining an appropriate imaging condition for TRM is challenging without knowledge of absolute time. Many experiments rely on scanning propagation-time movies to visually identify focusing (Allmann and Shearer, 2007), while the development of algorithmic imaging conditions is an active area of research. Steiner et al. (2008) suggest producing an image, i, via the maximum particle velocity over all time

$$i(x,z) = \max_t \sqrt{u_j(x,z,t)^2}, \qquad (1)$$

where subscript j is a summation index over the multi-component wave field $\mathbf{u}$. Further measures calculated on P and S-wave energy density wave fields are explored in Steiner (2009).

Figure 2 shows traces from TRM images calculated from an explosive point source in a homogeneous medium. As such there is only a P-wave component to this data volume. All panels show traces approaching the lateral position of the source as a function of depth after applying various imaging conditions. Panel a is the result produced by extracting the maximum over all time. Panel b is the square of panel a. Panel c is the zero lag of the autocorrelation over the time axis. Panels b and c are almost identical, which highlights the similarity of the imaging conditions as discussed in terms of vector norm definitions in Artman and Podladtchikov (2009). The two results to the right have a tighter depth response. Also, the ratio of the focus amplitude to the background value (signal-to-noise) has improved by 5 times since the background level is 0.2 in panel a, and 0.04 in panels b and c.

Kinematically, the amplitude maximum (l_∞ norm) of a vector and the sum of the squared vector (l_1) are the same for a

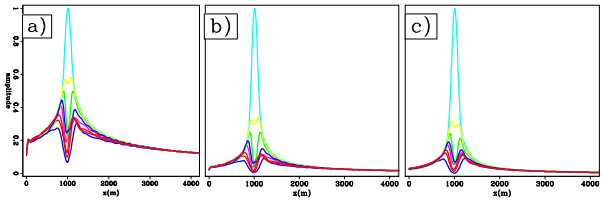

Figure 2 Amplitude-depth traces from TRM images due to a single point source in homogeneous background. Panel a) used $\max_t$, b) is $\max_t^2$, and c) is the zero lag of the autocorrelation.

simple transient point source. However, there are three advantages to imaging via correlations. First, the result is physically meaningful since it has units proportional to energy. Second, squaring emphasizes the focus above background levels by penalizing small numbers. Last, complicated source functions with long codas will be collapsed via autocorrelation. In contrast, imaging with the $\max_t$ only uses the most energetic, or dominant, portion of the function for imaging. For minimum-phase source functions this makes no difference. However, if the energy of the coda is large or larger than that contained in the dominant arrival, the autocorrelation will have a signal-to-noise ratio (SNR) improvement compared to the $\max_t$ image. For a random function, the improvement would be proportional to the square-root of the time duration of the source function.

MULTICOMPONENT REFLECTOR IMAGING

An extension of the "exploding reflector" concept (Claerbout, 1985), or the "exploding (mode) converter," can be used to understand imaging schemes for migrating compressional to shear (P-S) converted reflections with separate acoustic propagators. To do so, wave-field decomposition must be performed in the data space, or on the acquisition plane (Zhe and Greenhalgh, 1997; Dellinger et al., 2001). Coupling between the shear and compressional wave fields is subsequently introduced in the imaging condition via a correlation of the two wave fields. This is effectively a single-scattering representation of the complete wave equation.

With a modest increase in computational burden, the full elastic solution to the wave equation can be implemented as opposed to the far-field acoustic approximations routinely utilized. So doing removes the need for approximate surface processing of the raw data to separate P and S energy within the records. This allows wave-field decomposition during the imaging stage in the model domain. Performing the decomposition in the model domain after extrapolation ensures a regular and complete domain that does not require approximations for the vertical derivative (Huang and Milkereit, 2007).

Fortunately, only two simple vector identities are needed to separate P and S energy exactly since the displacement wave field, $\mathbf{u}(x,t)$, can be described as the sum of Helmholtz potentials (HP). Capitalizing on the facts that the curl of the irrotational HP is zero and the divergence of the solenoidal HP is zero, the compressional, E_p, and shear, E_s, kinetic energies are (Morse and Feshbach, 1953)

$$E_P = \quad P^2 \quad = (\lambda + 2\mu)(\nabla \cdot \mathbf{u})^2 \tag{2}$$

$$E_s = \quad S^2 \quad = \mu(-\nabla \times \mathbf{u})^2, \tag{3}$$

where the Lame coefficients λ and μ scale the amplitude of the results. The wave fields P and S have preserved sign information that captures the relative energy amplitudes within the two propagation modes (Dougherty and Stephen, 1988). The correlation type combination of the wave field components P and S to image the mode-converted reflections in active seismic data is (Wapenaar et al., 1987; Yan and Sava, 2008)

$$I_{ps}(\mathbf{x}) = \sum_t P_d(\mathbf{x},t) S_u(\mathbf{x},t) \;, \tag{4}$$

where subscripts d and u refer to extraction of the HP's from the down-going and up-coming wave fields.

Shragge et al. (2006) introduced imaging forward scattered mode conversions in teleseismic data by simply changing the causality of the source propagation, which effectively changes P_d above to P_u. The forward scattering (one-way) P to S imaging condition can also be interpreted as the location of an oriented source, which leads to the concept of imaging an actual "explosion" instead of the "exploding reflector."

ELASTIC TRM IMAGING CONDITIONS

An oriented subsurface source instigates both P and S waves that separate in the far field where they are recorded. In reality, there are P and S-wave surfaces similar to that shown in Figure 1 that are coincident only at the source location. The vector identities provided by equations 2 and 3 eliminate the need to characterize the source and process the data before imaging by exactly separating the two cones into individual wave fields. By finding the model coordinates where the P and S energy is collocated, we identify the source location.

We propose several elastic imaging conditions for locating subsurface sources that exploit the ability to propagate the entire wave field, and separate P and S components within the model domain. The two potentials can be considered independently via autocorrelation, or combined with cross-correlation. The method which produces the optimal image also contains valuable information about the source mechanism. The TRM imaging condition for locating body wave generators such as an oriented point source is (Artman et al., 2009)

$$i_b(\mathbf{x}) = \sum_t P_u(\mathbf{x},t) S_u(\mathbf{x},t). \tag{5}$$

Subscript b refers to the assumption that P and S body waves are produced by the source. Note the similarity to equation 4 with the important difference that both potentials are extracted from the up-coming wave field. Secondary sources (diffractors) are sources within this context and are also imaged. Similar images calculated from the auto-correlations, i_P and i_S can easily be constructed.

The global algorithm is a chain of: propagation, decomposition, and correlation. A time-domain finite-difference solution

to the elastic wave equation is used for propagation (Saenger et al., 2000). Multicomponent time-reversed data are source functions for the outer time loop. Wave field decomposition and correlations are performed for each time step. Because only the zero lag of the correlations are required, the image is simply calculated by accumulating the product of wave fields at every extrapolation step.

Figure 3 shows the collapse of energy from a vertical point source at depth recorded at the surface via reverse propagation of the elastic wave field. The panels are all extracted from the extrapolation time axis at the initiation time of a vertical point source. Panel a is the sum of the squares of the Cartesian displacement components. Panels b and c are the P and S-wave potentials respectively. The source is located at the maximum amplitude of panel a and at the zero crossings in the center of panels b and c. Longer wavelengths are seen on the P image due to faster propagation velocity. The extra events on panel b are the limited aperture artifacts. The hyperbola on panel c is a downward propagating P-S conversion from the free surface. The linear events are nonphysical artifacts associated with using the data as displacement sources(Yan and Sava, 2008).

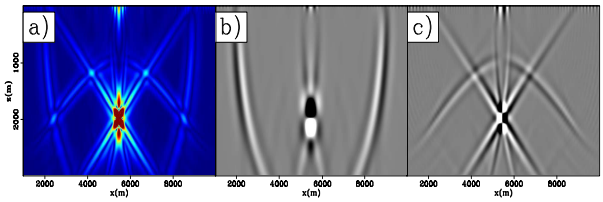

Figure 3 Absolute particle velocity, P, and S wave fields in (x,z) after reverse propagating to the initiation time of a vertical point source.

Figure 4 shows the zero lag of the autocorrelations of P and S energy and their cross correlation after reverse propagating the forward modeled data. While the autocorrelations are strictly positive, the correlation of the P and S wave fields has zero mean. The source location in panel c is at the location of a zero crossing, thereby having an amplitude identical (or similar) to most of the rest of the domain. The anti-symmetric clover-leaf pattern surrounding the source identifies its location. For unknown source functions, computing all three images will provide polarization information about the source function as well as location.

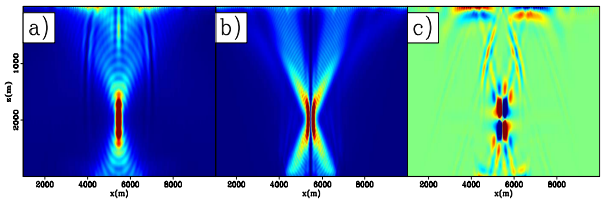

Figure 4 Auto and cross-correlations of component wave fields imaging a vertical point source by TRM with an elastic propagator. Panels a,b and c are *PP*, *SS*, and *PS* respectively.

The asymmetry revealed in the impulse response of the mode cross-correlation imaging condition in Figure 4c suggests simple post-processing to identify the source position with an energy anomaly instead of the multidimensional zero crossing seen in the image. The spatial integral or derivative of the image in panel c will provide a $\pm 90^o$ phase roll in the image that will locate the source with a maximum.

IMAGING MANY SOURCES

Figure 5a shows a realistic velocity model used to forward model a complex source location experiment. Constant V_p/V_s ratio and density were used. The receiver stations used for TRM are indicated by the circles at the top of panels b and c. The modeled data were produced with a swarm of randomly triggered point sources with Ricker wavelet time functions, central frequency 4.5 Hz. Panel b is the TRM image with correlation imaging condition of the P and S wave fields (equation 5).

Simultaneously imaging the direct arrivals of many sources distributed over space and time introduces a-physical cross talk into the image. If the sources are random time signals that are minimally correlatable, the cross talk is minimized. However, it is not likely that a swarm of subsurface sources related to the same mechanism will have substantially different time signatures. Therefore, the forward modeling always uses the same Ricker wavelets, but allows a single source location to be excited randomly 1 to 3 times with varying amplitude during the 10 seconds of data. The $\max_t$ imaging condition would only keep focus locations due to the strongest events whereas the correlation approach will keep energy from all constituents.

Despite the near-surface jitter and cross-talk artifacts in panel b, the image due to the source swarm produces a feature resembling the antisymmetric cloverleaf seen in the impulse response image in Figure 3c. Knowing that the impulse response of a point source identifies the source location at the multidirectional zero-crossing motivates applying a spatial integral to the image result. While the derivative of the image provides a higher wavenumber image for simple data volumes, the global nature of the integral is much more stable for images produced with complex data wave fields. Figure 5c is the integration of panel b with the source locations overlain.

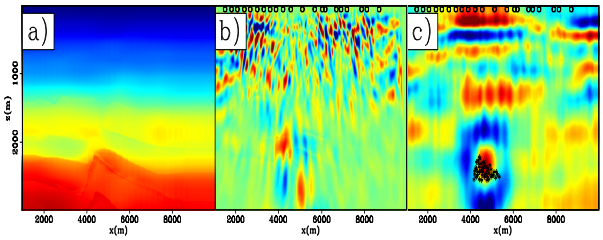

Figure 5 Velocity model and P-S body-wave TRM images before (b) and after (c) spatial integral. Receiver and source locations overlain.

CONCLUSIONS

When recording the full wave field in any geophysical experiment, it is logical to use fully elastic propagators for a migration or focusing algorithm. Especially in the case of event location, the TRM algorithm benefits from elastic propagators since sufficient characterization of the source may be impossible for wave field decomposition at the acquisition plane. This is particularly important for sources that are not transient in nature or compact in time.

We use the chain of elastic propagation, wave field decomposition, and correlation imaging (defined as migration) to image source locations. In this application the critical time differences used for imaging are extracted from the time delay between P and S-wave travel paths. The algorithm is both a refinement of time-reverse modeling and could be appropriately included within the general definition of migration.

Physical interpretation of the back-propagated data is extracted by applying imaging conditions designed to extract particular kinematic events within the data. For the case of locating subsurface sources, the imaging condition we have selected is the correlation of the P and S-wave energy. In the forward scattering (one-way travel path) observation of non-explosive sources, the energy partition between compressional and shear waves is only collocated at the physical origin of the source. The methodology is sufficiently robust to tolerate irregular acquisition geometry and multiple sources in the wave field.

REFERENCES

Allmann, B. P. and P. M. Shearer, 2007, A high-frequency secondary event during the 2004 parkfield earthquake: Science, **318**, 1279–1284.

Artman, B. and I. Podladtchikov, 2009, Imaging conditions for time-reverse acoustics: Workshop on passive seismic, Expanded Abstracts, 168–174, EAGE.

Artman, B., I. Podladtchikov, A. Goertz, B. Steiner, and E. H. Saenger, 2009, Imaging the exploding converter with elastic propagators: Presented at the 71st Conference and Exhibition, EAGE.

Claerbout, J., 1985, Imaging the Earth's interior: Blackwell Scientific Publications.

Dellinger, J. A., B. Nolte, and J. T. Etgen, 2001, Alford rotation, ray theory, and crossed-dipole geometry: Geophysics, **66**, 637–647.

Dougherty, M. E. and R. A. Stephen, 1988, Seismic energy partitioning and scattering in laterally heterogeneous ocean crust: Pure and Applied Geophysics, **128**, 195–229.

Fink, M., 1999, Time-reversed acoustics: Scientific American, **November**, 67–73.

Gajewski, D. and E. Tessmer, 2005, Reverse modelling for seismic event characterization: Geophys. J. Int., **163**, 276–284.

Huang, J. and B. Milkereit, 2007, Wave-equation-based separation of p- and s-wave modes: SEG Technical Program Expanded Abstracts, **26**, 2135–2139.

Levin, S. A., 1984, Principle of reverse-time migration: Geophysics, **49**, 581–583.

Morse, P. M. and H. Feshbach, 1953, Methods of theoretical physics: McGraw-Hill Book Company. (New York).

Saenger, E. H., N. Gold, and S. A. Shapiro, 2000, Modeling the propagation of elastic waves using a modified finite-difference grid: Wave Motion, **31**, 77–92.

Shragge, J. C., B. Artman, and C. Wilson, 2006, Teleseismic shot-profile migration: Geophysics, **71**, SI221–SI229.

Steiner, B., 2009, Time reverse modeling of low-frequency tremor signals: PhD thesis, Swiss Federal Institute of Technology Zurich, **18268**.

Steiner, B., E. H. Saenger, and S. M. Schmallholz, 2008, Time reverse modeling of low-frequency microtremors: Application to hydrocarbon reservoir localization: Geophysical Research Letters, **35**, L03307.

Wapenaar, C. P. A., N. A. Kinneging, and A. J. Berkhout, 1987, Principle of prestack migration based on the full elastic two-way wave equation: Geophysics, **52**, 151–173.

Yan, J. and P. Sava, 2008, Isotropic angle-domain elastic reverse-time migration: Geophysics, **73**, S229–S239.

Zhe, J. and S. A. Greenhalgh, 1997, Prestack multicomponent migration: Geophysics, **62**, 598–613.